Kinetics of the Unimolecular Decomposition of the C_2Cl_3 Radical

Mikhail G. Bryukov,† Sofya A. Kostina, and Vadim D. Knyazev*

Research Center for Chemical Kinetics, Department of Chemistry, The Catholic University of America, Washington, D.C. 20064

Received: January 24, 2003; In Final Form: May 8, 2003

The $C_2Cl_3 \rightarrow C_2Cl_2 + Cl$ (1) reaction was studied using the laser photolysis/photoionization mass spectrometry technique. Rate constants were determined in time-resolved experiments as a function of temperature (569−683 K) and bath gas density ([He] = (3−24) × 10^{16} atoms cm^{-3}, [N_2] = 12 × 10^{16} molecules cm^{-3}). C_2Cl_2 was observed as a primary product of reaction 1. Rate constants of reaction 1 are in the falloff, closer to the low-pressure limit, under the conditions of the experiments. The potential energy surface (PES) of reaction 1 was studied using a variety of quantum chemical methods. The results of the PES study indicate that the minimum energy path of the C_2Cl_3 dissociation proceeds through a shallow-well symmetric structure with the departing Cl atom equidistant from both carbon atoms; a PES saddle point exists between the nonsymmetric equilibrium C_2Cl_3 structure and the symmetric one. The results of quantum chemical calculations and the experimental rate constant data were used to create a model of reaction 1. The experimental dependence of the rate constant of C_2Cl_3 decomposition on temperature and pressure was reproduced in RRKM/master equation calculations. The reaction model provides expressions for the temperature dependences of the high-pressure-limit and the low-pressure-limit rate constants and the falloff broadening factors: $k_1^{\infty} = (1.36 \times 10^{13})T^{0.29} \exp(-13625\ K/T)\ s^{-1}$, $k_1°(He) = (4.89 \times 10^{12})T^{-6.14} \exp(-14497\ K/T)\ cm^3\ molecule^{-1}\ s^{-1}$, $k_1°(N_2) = (1.525 \times 10^{12})T^{-5.95} \exp(-14393\ K/T)\ cm^3\ molecule^{-1}\ s^{-1}$, $F_{cent}(He) = 0.33 \exp(-T/1836\ K) + 0.67 \exp(-T/98\ K) + \exp(-3650\ K/T)$, and $F_{cent}(N_2) = 0.35 \exp(-T/1864\ K) + 0.65 \exp(-T/103\ K) + \exp(-3614\ K/T)$. The experimental data are not sufficient to specify all the parameters of the model; consequently, some of the model parameters were obtained from quantum chemical calculations and from analogy with other reactions of radical decomposition. Thus, the parametrization is most reliable under conditions close to those used in the experiments.

I. Introduction

Kinetic modeling of processes such as combustion and incineration of chlorinated hydrocarbons and industrial chlorination is essential for understanding their mechanisms and for use of these mechanisms as tools of prediction and control. The success of such modeling is currently limited by a lack of fundamental information on the rates and products of a large number of elementary reactions involving chlorinated hydrocarbon radicals.[1] Reactions of the trichlorovinyl radical, C_2Cl_3, have been demonstrated to be among the most important and sensitive reactions in a number of systems of combustion and pyrolysis of chlorine-rich unsaturated chlorinated hydrocarbons.[2−4] The principal reactions responsible for C_2Cl_3 removal are its reaction with O_2, thermal decomposition, and reaction with molecular chlorine. The $C_2Cl_3 + O_2$ reaction has been studied experimentally.[5] The rate constants of the reaction of C_2Cl_3 radical with molecular chlorine were recently determined by us in direct, time-resolved experiments.[6] The kinetics of the thermal decomposition of C_2Cl_3, however, remains unknown: no experimental or theoretical information on this reaction is currently available in the literature.

In this paper, we report the results of our experimental investigation of the reaction of the thermal unimolecular decomposition of the C_2Cl_3 radical:

$$C_2Cl_3 \rightarrow C_2Cl_2 + Cl \qquad (1)$$

Reaction 1 was studied in the 569−683 K temperature interval at varying densities of the helium bath gas ([He] = (3−24) × 10^{16} atoms cm^{-3}) and at one density of nitrogen bath gas ([N_2] = 12 × 10^{16} molecules cm^{-3}). The experimental study is described in the next section. Section III presents a quantum chemical computational study of the potential energy surface, an RRKM/master equation model of the reaction, and a parametrized representation of the calculated rate constants over wide ranges of temperatures and pressures. A discussion of the experimental and the computational results is given in section IV.

II. Experimental Study and Results

II.1. Experimental Apparatus and Method. Trichlorovinyl radicals were produced by the pulsed, 248 nm laser photolysis of tetrachloroethylene:[5]

$$C_2Cl_4 \xrightarrow{248\ nm} C_2Cl_3 + Cl$$
$$\rightarrow \text{other products} \qquad (2)$$

The decay of C_2Cl_3 was subsequently monitored in time-resolved experiments using photoionization mass spectrometry. Details of the experimental apparatus[7] and procedures[8] used have been described before and thus are only briefly reviewed here.

Pulsed unfocused 248 nm radiation (4 Hz) from a Lambda Physik EMG 201MSC excimer laser was directed along the axis

* To whom correspondence should be addressed. E-mail: knyazev@cua.edu.

† Current address: Biodynamics Institute, Louisiana State University, 711 Choppin Hall, Baton Rouge, LA 70803.

10.1021/jp034205g CCC: $25.00
Published on Web 07/31/2003

of a heatable quartz or Pyrex reactor (1.05 cm i.d., coated with boron oxide[9] or uncoated). Gas flowing through the tube at ~4 m s^{-1} contained the radical precursor (≤0.01%) and an inert carrier gas (He or N_2) in large excess. The flowing gas was completely replaced between laser pulses.

Gas was sampled through a hole (0.04 cm diameter) in the side of the reactor and formed into a beam by a conical skimmer before the gas entered the vacuum chamber containing the photoionization mass spectrometer. As the gas beam traversed the ion source, a portion was photoionized and mass selected. C_2Cl_3, C_2Cl_2, and C_2Cl_4 were ionized using the light from a hydrogen resonance lamp (10.2 eV). Temporal ion signal profiles were recorded on a multichannel scaler from a short time before each laser pulse up to 25 ms following the pulse. Typically, data from 1000−10000 repetitions of the experiment were accumulated before the data were analyzed.

The gases used were obtained from Aldrich (C_2Cl_4, >99%) and MG Industries (He, > 99.999%; N_2, > 99.999%). C_2Cl_4 was purified by vacuum distillation prior to use. Helium and nitrogen were used as provided.

The C_2Cl_3 ion signal profiles were fit to an exponential function ($[C_2Cl_3]_t = [C_2Cl_3]_0 e^{-k't}$) using a nonlinear least-squares procedure. Unimolecular decay of C_2Cl_3 was observed only above 500 K. Below this temperature a slow decay of C_2Cl_3 is observed due to a first-order heterogeneous wall-loss process:

$$C_2Cl_3 \rightarrow \text{heterogeneous loss} \qquad (3)$$

Above 500 K the decay constant increased rapidly with rising temperature due to the increasing importance of the thermal decomposition of C_2Cl_3 radical, reaction 1. The decay constants were analyzed assuming that C_2Cl_3 radicals were consumed only by two elementary reactions, 1 and 3. At low temperatures, only the heterogeneous loss is observed ($k' = k_3$). Above 500 K the sum of the two loss processes is observed ($k' = k_1 + k_3$).

Calculations of k_1 from measurements of k' require knowledge of k_3 above 500 K. While k_3 was directly determined below 500 K (13−29 s^{-1}, independent of temperature between 370 and 500 K), it could not be measured above this temperature due to the additional loss of radicals by unimolecular decomposition. Values of k_3 above 500 K needed to determine k_1 from the measurements of k' were obtained by an extrapolation assuming that k_3 retains its temperature independence beyond 500 K up to the highest temperature of this study, 683 K. To minimize possible errors in the determination of k_1 caused by this assumed temperature independence of k_3 above 500 K, experiments to obtain k_1 were conducted at temperatures sufficiently high to ensure that $k' \geq 2.5k_3$. It was this criterion that established the lowest temperature used to determine k_1 at each bath gas density. The highest temperature used at each total gas density was determined by the fact that decay constants above 600 s^{-1} could not be measured accurately. The limitations in the temporal resolution of the experimental apparatus are determined by two factors: the finite time of radial diffusion of the radicals under study and the effects of molecular velocity distribution on time-resolved mass spectrometric sampling.[10]

Experiments were performed to establish that the rate constants did not depend on the concentration of precursor (provided that the concentration was kept low enough to ensure that radical−radical reactions had negligible rates), reactor wall material, or the photolyzing laser intensity. The rate constants of the C_2Cl_3 decomposition depended only on temperature and bath gas density.

II.2. Experimental Results. The results of all the experiments and the conditions used to determine k_1 are given in Table 1.

TABLE 1: Conditions and Results of Experiments To Determine the Rate Constants k_1 of the Unimolecular Decomposition of C_2Cl_3

[M][a]	T/K	$[C_2Cl_4]$[b]	$[C_2Cl_3]_0$[c]	I[d]	k_3/s^{-1}	k_1[e]/s^{-1}
			He Bath Gas			
3.02	609	10	19	100	20.5	32.5 ± 4.1
3.03	619	20	39	100	20.0	42.3 ± 4.3
3.03	629	10	20	100	20.5	68.5 ± 5.7
3.03	639	20	40	100	20.0	83.5 ± 5.6
3.03	649	10	20	100	20.5	109.3 ± 7.3
3.03	659	20	41	100	20.0	144.6 ± 6.6
3.03	668	10	21	100	20.5	165 ± 11
3.03	683	20	41	100	20.0	260 ± 11
6.04	590	4.1	8.4	108	14.3	30.6 ± 2.4
6.05	600	10	21	108	19.4	44.2 ± 2.6
6.04	610	4.1	8.6	108	14.3	60.0 ± 2.9
6.05	619	10	21	108	19.4	75.6 ± 3.6
6.05	629	4.1	8.8	108	14.3	103.2 ± 5.8
6.05	639	10	22	108	19.4	143.1 ± 4.1
6.05	649	10	22	108	19.4	185.2 ± 5.5
6.05	659	10	22	108	19.4	220.6 ± 7.1
6.05	669	10	22	108	19.4	294.1 ± 8.0
12.1	575	7.2	13	100	18.8	34.9 ± 1.6
12.0	583[f]	5.5	10	100	17.8	47.4 ± 2.2
12.1	585	7.2	14	100	18.8	50.7 ± 2.0
12.1	590	3.6	6.8	100	12.7	59.7 ± 2.0
12.1	591	16	8.1	27	15.8	54.4 ± 2.0
12.0	593[f]	5.5	11	100	17.8	58.7 ± 2.2
12.0	602[f]	5.5	11	100	19.0	96.0 ± 2.5
12.1	603	7.2	14	100	18.8	88.9 ± 2.7
12.1	610	3.6	7.0	100	12.7	102.2 ± 2.8
12.1	611	16	8.3	27	15.8	106.0 ± 3.1
12.1	622	7.2	14	100	18.8	154.2 ± 3.2
12.0	622[f]	5.5	11	100	19.0	162.9 ± 3.4
12.1	630	3.6	7.2	100	12.7	202.7 ± 4.2
12.1	630	16	8.5	27	15.8	191.6 ± 2.5
12.0	632[f]	5.5	11	100	19.0	215.0 ± 4.3
12.0	632[f]	5.5	11	100	19.0	212.0 ± 5.1
12.1	642	7.2	15	100	18.8	259.8 ± 7.9
12.0	642[f]	5.5	11	100	19.0	292.4 ± 7.0
12.1	649	3.6	7.3	100	12.7	345.0 ± 9.4
12.1	650	16	8.7	27	15.8	326.2 ± 6.5
12.0	652[f]	5.5	11	100	19.0	373.8 ± 7.8
12.1	659	3.6	7.3	100	12.7	436.2 ± 9.2
12.1	660	16	8.8	27	15.8	427.7 ± 6.7
24.2	569	8.0	16	108	18.4	55.8 ± 2.4
24.3	579	30	17	30	23.9	65.6 ± 3.7
24.3	589	8.0	16	108	18.4	98.5 ± 4.0
24.2	599	30	17	30	23.9	138.3 ± 4.7
24.2	609	8.0	17	108	18.4	186 ± 10
24.2	619	30	18	30	23.9	263 ± 17
24.2	629	8.0	17	108	18.4	340 ± 17
24.2	639	30	18	30	23.9	463 ± 26
24.2	649	8.0	18	108	18.4	555 ± 23
			N_2 Bath Gas			
12.1	609	21	41	100	29.4	138 ± 10
12.0	610	13	24	93	16.4	150 ± 9
12.0	625	13	24	93	16.4	220 ± 11
12.1	629	21	42	100	29.4	225 ± 15
12.0	639	13	24	93	16.4	306 ± 17
12.1	639	21	42	100	29.4	315 ± 23
12.0	654	13	25	93	16.4	499 ± 32

[a] Concentration of the bath gas (helium or nitrogen) in units of 10^{16} atoms cm^{-3} or molecules cm^{-3}. [b] In units of 10^{11} molecules cm^{-3}. [c] In units of 10^{10} molecules cm^{-3}. The C_2Cl_3 concentrations were obtained by measuring the photolytic depletion of C_2Cl_4 and represent an upper limit since they were obtained assuming a 100% yield of C_2Cl_3 in the photolysis. [d] Estimated photolyzing laser intensity in mJ $pulse^{-1}$ cm^{-2}. [e] Error limits represent 1σ statistical uncertainty. [f] A quartz reactor coated with boron oxide was used. An uncoated Pyrex reactor was used in all other experiments.

The unimolecular rate constants for reaction 1 obtained from these sets of experiments conducted at four different densities

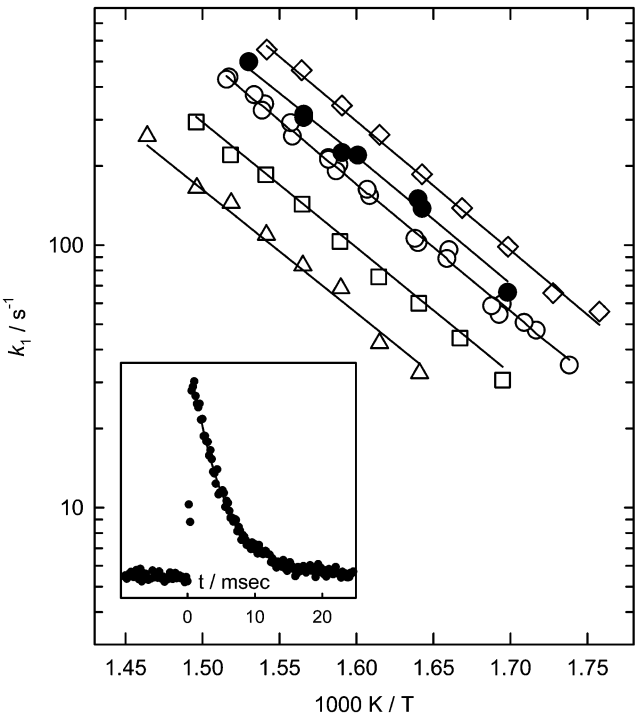

Figure 1. C_2Cl_3 decomposition rate constants (k_1 vs 1000/T) for four densities of helium (open symbols) and one density of nitrogen (filled circles). Lines represent the results of master equation simulation. Key: triangles, [He] = 3×10^{16} atoms cm^{-3}; squares, [He] = 6×10^{16} atoms cm^{-3}; circles, [He] = 12×10^{16} atoms cm^{-3} and [N_2] = 12×10^{16} molecules cm^{-3}; tilted squares, [He] = 24×10^{16} atoms cm^{-3}. The inset shows an example of the C_2Cl_3 decay profile: [He] = 12.1×10^{16} atoms cm^{-3}, T = 630 K, k' = 207 s^{-1}.

of helium ($(3-24) \times 10^{16}$ atoms cm^{-3}) and one density of nitrogen (12×10^{16} molecules cm^{-3}) are shown in Figure 1. The C_2Cl_3 detection sensitivity was lower when nitrogen was used as a bath gas, and k_1 values in this case could be determined only under optimal conditions. Error limits of the k_1 values in Table 1 represent 1σ statistical uncertainty. Potential uncertainties associated with the assumed temperature independence of the wall decay of C_2Cl_3 are not easily evaluated. Therefore, no attempt was undertaken to quantify their contribution.

The values of k_1 increase with pressure; the k_1 vs pressure dependence at each particular temperature is somewhat weaker than proportional. Thus, reaction 1 is in the falloff region under the conditions of the current study, relatively close to the low-pressure limit. C_2Cl_2 was observed as a primary product of reaction 1 with the C_2Cl_2 characteristic rise time matching that of the C_2Cl_3 decay due to thermal decomposition. No other potential primary or secondary products were observed.

III. Model of Reaction 1

III.1. Potential Energy Surface. The potential energy surface (PES) of the reactive system of C_2Cl_3 decomposition and the corresponding reverse reaction, that of addition of Cl to the triple bond of C_2Cl_2, was studied using four combinations of methods and basis sets: UMP2/6-31G(d), UMP2/6-311G(2d), BH&HLYP/6-31G(d), and QCISD/6-31G(d). In addition, higher level single-point calculations were performed at selected critical points using the QCISD(T)[11] method with the large 6-311+(3df) basis set. A description of the methods and the basis sets can be found in ref 12. The version of the BH&HLYP functional[13,14] implemented in the Gaussian 98[15] suite of programs (used in all quantum chemical calculations) was used. Two-dimensional scans of the PES were performed at the UMP2/6-31G(d) and

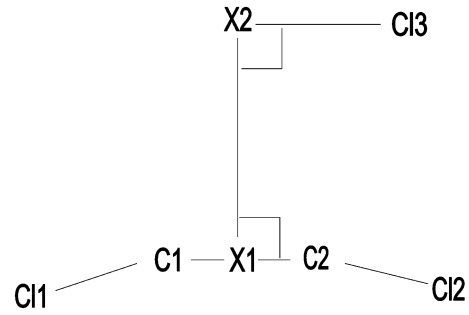

Figure 2. System of coordinates used in the study of the potential energy surface of reaction 1 (see the text).

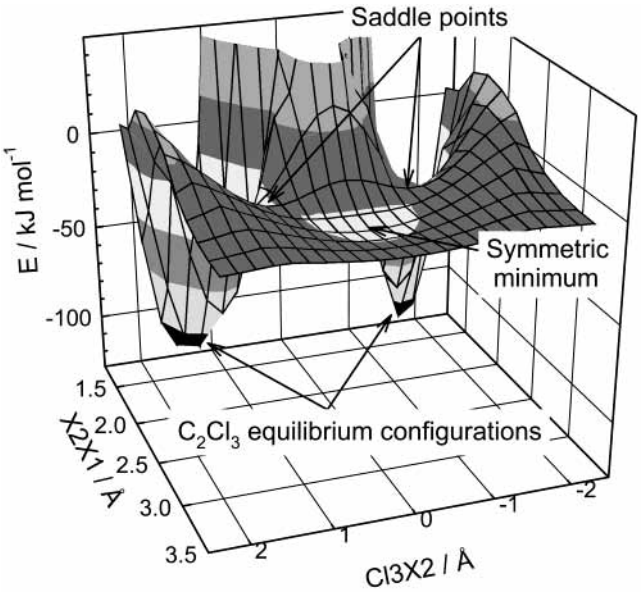

Figure 3. Three-dimensional surface plot obtained in a relaxed scan of the PES of reaction 1 using the BH&HLYP/6-31G(d) method. The minimum energy path of the C_2Cl_3 dissociation proceeds from one of the nonsymmetric minima (C_2Cl_3 equilibrium configurations) through a corresponding saddle point and the symmetric shallow-well minimum.

the BH&HLYP/6-31G(d) levels. The system of coordinates employed in these scans is shown in Figure 2. Point X1 (pseudoatom) was positioned in the middle of the C−C bond, and point X2 was placed at the intersection of two lines: one line passing through X1 and perpendicular to the C−C bond and the other line passing through the Cl3 (departing) atom and parallel to the C−C bond. The X1−X2 and the Cl3−X2 distances were scanned with the rest of the coordinates optimized.

The results of the UMP2/6-31G(d) and the BH&HLYP/6-31G(d) scans are in qualitative agreement. The PES obtained in the BH&HLYP/6-31G(d) scan is displayed in Figure 3. Three minima are observed on the PES: two identical minima corresponding to the equilibrium configuration of C_2Cl_3 and one shallow minimum corresponding to a symmetrical structure with the departing Cl3 atom equidistant from both C atoms. The equilibrium nonsymmetrical minima are separated from the symmetrical minimum by saddle points.

The minimum energy path for C_2Cl_3 decomposition thus proceeds from the nonsymmetric equilibrium structure of C_2Cl_3 through a saddle point to the shallow symmetric minimum, with subsequent departure of Cl via a symmetric pathway (Cl equidistant from both C atoms). To ascertain the existence of the saddle point on the nonsymmetric → symmetric reaction path, additional calculations were performed. Structures of the

TABLE 2: Energies[a] of Critical Points on the PES of the $C_2Cl_3 \rightarrow Cl + C_2Cl_2$ Reaction Obtained in Quantum Chemical Calculations

	structure		
computational method	saddle point	symmetric minimum	$Cl + C_2Cl_2$
BH&HLYP/6-31G(d) (optimization)	102.88	99.98	112.70
ZPE contribution[b]	−4.50	−3.32	−3.90
MP2/6-311G(2d) (optimization)	91.86	50.89	62.56
PMP2/6-311G(2d)//MP2/6-311G(2d)	84.72	74.90	87.43
QCISD(T)/6-311+G(3df)//MP2/6-311G(2d)	98.22	91.21	103.96
ZPE contribution[b]	−2.58	−4.09	−7.68
QCISD/6-31G(d) (optimization)	103.25	91.39	94.82
QCISD/6-311+G(3df)//QCISD/6-31G(d)	99.55 (99.66)[d]	98.15	109.95
ZPE contribution[b]	−5.04	−6.31	−6.73
experiment[c]	109.8 ± 6.7		

[a] Energy values are given in units of kJ mol^{-1} relative to the C_2Cl_3 equilibrium configuration, with ZPE included. [b] Contribution of the zero-point energy (included in the energy values above) calculated at the level of theory used for geometry optimization. [c] Value of the energy barrier derived from modeling of the experimental data performed in this study (section III). [d] The value in parentheses was obtained using the IRCmax method[38,39] with a step size of 0.1 $amu^{1/2}$ bohr.

C_2Cl_3 nonsymmetric equilibrium configuration, saddle point, symmetric C_2Cl_3 configuration, and $Cl + C_2Cl_2$ products were calculated using the UMP2/6-311G(2d), BH&HLYP/6-31G(d), and QCISD/6-31G(d) methods. Vibrational frequencies of all critical points were obtained at the optimized structures. Higher level QCISD(T)/6-311+(3df) single-point energy values were calculated for all these critical points using the UMP2- and the QCISD-optimized structures, and the contributions of the ZPE were included. The results are presented in Table 2. As can be seen from the data, all calculations result in the saddle point energy being higher than that of the shallow symmetric minimum. Also, the BH&HLYP/6-31G(d) and the QCISD(T)/6-311+(3df) calculations result in the saddle point energy being lower than that of the $Cl + C_2Cl_2$ products. The detailed results of quantum chemical calculations are presented in the Supporting Information.

III.2. Rate Constant Calculation. A model of reaction 1 was created on the basis of the results of quantum chemical calculations and the experimental data of the current study. QCISD/6-31G(d)-level structures and frequencies were used for all species. The saddle point connecting the nonsymmetric equilibrium C_2Cl_3 structure and the symmetric shallow minimum was taken as the dynamic bottleneck (transition state) of the reaction. This is a reasonable assumption considering the fact that further chemical transformation of the symmetric structure can be expected to largely favor dissociation via a very "loose" [16] complex rather than reassociation to form C_2Cl_3 through a "tighter" transition state.

Microcanonical energy-dependent rate constants for C_2Cl_3 decomposition ($k(E)$) were calculated using the RRKM method.[17−20] The sum-of-states and the density-of-states functions of the transition state and the C_2Cl_3 molecule, respectively, were calculated using the modified Beyer−Swinehart algorithm.[21] One rotational degree of freedom in both the transition state and the C_2Cl_3 molecule was taken as active.[17−20] To approximately account for the conservation of angular momentum, $k(E)$ values were multiplied by the ratio of the moments of inertia of the remaining adiabatic rotational degrees of freedom.

Pressure- and temperature-dependent rate constants of C_2Cl_3 decomposition were calculated via solution of a steady-state master equation[19] using the Nesbet algorithm.[22] It was demonstrated that the calculated rate constant values did not depend on the size of the energy increment (30 cm^{-1} used in master equation solution with 5 cm^{-1} used in $k(E)$ calculations) used in converting the continuous form of the master equation into the matrix form.[19] It was also demonstrated that solution of the full time-dependent master equation[19] performed using the Householder tridiagonalization algorithm (see refs 23 and 24 for details) resulted in the same rate constant values that were obtained with the steady-state master equation. The ChemRate program[25] was used in all calculations.

The exponential-down[19,26] model of collisional energy transfer was used in the calculations. The values of the collisional energy transfer parameter, $\langle\Delta E\rangle_{down}$ (average energy transferred per deactivating collision with the bath gas), is unknown and can only be obtained from fitting of the experimental data. However, this parameter, generally, has unknown temperature dependence. The model of the $\langle\Delta E\rangle_{down}$ vs temperature dependence for C_2Cl_3 used here was based on analogy with the results of Knyazev and Tsang obtained for *sec*-C_4H_9.[27] These authors modeled the chemically and thermally activated decomposition of *sec*-C_4H_9 to reproduce the experimental literature data obtained over a wide range of temperatures (195−680 K). The modeling yielded $\langle\Delta E\rangle_{down}$ proportional to temperature: $\langle\Delta E\rangle_{down}$(*sec*-$C_4H_9$,He) $= 0.52T$ cm^{-1} K^{-1}. A similar proportional dependence was obtained earlier for the decomposition of ethyl radical.[28,29] Thus, a proportional dependence

$$\langle\Delta E\rangle_{down} = \alpha T \qquad \text{(I)}$$

was used in the model of reaction 1. Uncertainties resulting from this assumed form of the $\langle\Delta E\rangle_{down}$ vs T dependence were estimated by repeating selected parts of the modeling exercise using the temperature-independent $\langle\Delta E\rangle_{down}$ ($\langle\Delta E\rangle_{down}$ = constant).

The energy threshold of reaction 1 (E_1) and the coefficient α_{He} of the $\langle\Delta E\rangle_{down}$ vs T dependence for helium bath gas (eq I) were adjusted to reproduce the experimental values of $k_1(T,[He])$ obtained in the current study. Data fitting was performed by minimization of the weighted sum of squares of deviations. Each data point was assigned a weight equal to k_1^{-1}. Such weighting represents an intermediate case between an unweighted fit (which would give unfairly large weights to large rate constant values) and fitting "on a logarithmic scale" (minimizing the sum of squares of deviations of logarithms), which would treat relative deviations at low and high pressures equally. Considering the fact that low rate constant values are subject to larger uncertainties because of the extrapolated temperature independence of k_3 (see section II), we chose the reciprocal weighting method of data fitting, which gives some preference to larger values but takes low-value rate constants into account as well. The optimized values are $E_1 = 109.8$ kJ mol^{-1} and $\alpha_{He} = 0.338$ cm^{-1} K^{-1}. Data fitting for the experimental k_1

TABLE 3: Properties of the Model of Reaction 1

Vibrational Frequencies (cm^{-1})[a]
C_2Cl_3: 140, 210, 273, 402, 473, 618, 879, 943, 1751
transition state: 93, 180, 189, 321, 364, 506, 997, 2197
Rotational Constants[a]
C_2Cl_3: $B_A = 0.1225\ cm^{-1}$ (active),
$B_{B,C} = 0.04136\ cm^{-1}$ (adiabatic)
transition state: $B_A = 0.0925\ cm^{-1}$ (active),
$B_{B,C} = 0.03732\ cm^{-1}$ (adiabatic)
Reaction Barrier
$E_1 = 109.76\ kJ\ mol^{-1}$
Collisional Energy Transfer Parameters
$\langle\Delta E\rangle_{down}(He) = 0.338T\ cm^{-1}\ K^{-1}$
$\langle\Delta E\rangle_{down}(N_2) = 0.535T\ cm^{-1}\ K^{-1}$

[a] Vibrational frequencies and molecular structures were obtained in QCISD/6-31G(d) calculations.

TABLE 4: Results of Modeling of the Experimental $k_1(T,[He])$ Data with Modified Versions of the Model of Reaction 1

model version	optimized E_1/kJ mol^{-1}	optimized $\langle\Delta E\rangle_{down}$(He)/cm^{-1}
"central" model[a]	109.76	$0.338T$
$\langle\Delta E\rangle_{down}$ = constant[b]	112.93	309
two frequencies increased[c]	107.62	$0.296T$
two frequencies reduced[d]	112.06	$0.381T$

[a] QCISD/6-31G(d) frequencies; $\langle\Delta E\rangle_{down}$ is assumed to be proportional to T. [b] QCISD/6-31G(d) frequencies; $\langle\Delta E\rangle_{down}$ is assumed to be independent of T. [c] QCISD/6-31G(d) frequencies with the two lowest frequencies increased by a factor of 2; $\langle\Delta E\rangle_{down}$ is assumed to be proportional to T. [d] QCISD/6-31G(d) frequencies with the two lowest frequencies decreased by a factor of 2; $\langle\Delta E\rangle_{down}$ is assumed to be proportional to T.

values obtained in nitrogen bath gas was performed with the E_1 fixed at the optimum value determined from modeling the rate constant data for helium bath gas. The optimized coefficient of eq I for nitrogen is $\alpha_{N_2} = 0.535\ cm^{-1}\ K^{-1}$. Details of the optimized model of reaction 1 are presented in Table 3. The resultant calculated values of the rate constants are in good agreement with the experimental results (Figure 1).

Data fitting was then repeated with several modified versions of the model to approximately evaluate the influence of uncertainties in certain parameters of the model. First, calculations were performed with the $\langle\Delta E\rangle_{down}$ = constant model of collisional energy transfer. Second, data fitting was repeated with modified properties of the transition state: two lowest vibrational frequencies of the transition state were doubled in one case and divided by 2 in the other case. Since reaction 1 is relatively close to the low-pressure limit under the experimental conditions of the current study, the modeling results are not very sensitive to the properties of the transition state; thus, the changes in the model induced by the variations of the vibrational frequencies are not dramatic. Table 4 presents the results of these fitting exercises performed with the modified versions of the model. The overall resultant uncertainty (6.7 kJ mol^{-1}) in the value of the reaction threshold was estimated by adding the variations in the optimized E_1 value caused by the uncertainty of the $\langle\Delta E\rangle_{down}$ vs T dependence, that of the transition-state frequencies, and the 2σ statistical uncertainty of the fitting (1.2 kJ mol^{-1}).

III.3. Parametrization of the Rate Constants. We present here a parametrization of k_1 in helium and nitrogen, which provides rate constant values throughout the range of temperatures 300−1400 K and pressures 1 to 1×10^4 Torr. The modified Lindemann−Hinshelwood expression introduced by Gilbert et al.[30] was used. Values of k_1 in the above temperature and pressure intervals were calculated using the master equation/RRKM approach with the optimum model of the reaction presented above (Table 3). The following temperature dependences of the high- and the low-pressure-limit rate constants were obtained:

$$k_1^{\infty} = (1.36 \times 10^{13})T^{0.29} \exp(-13625\ K/T)\ s^{-1} \quad \text{(II)}$$

$$k_1^{\circ}(He) = (4.89 \times 10^{12})T^{-6.14} \exp(-14497\ K/T)\ cm^3\ molecule^{-1}\ s^{-1} \quad \text{(III)}$$

$$k_1^{\circ}(N_2) = (1.53 \times 10^{12})T^{-5.95} \exp(-14393\ K/T)\ cm^3\ molecule^{-1}\ s^{-1} \quad \text{(IV)}$$

The matrix of calculated values of rate constants was fitted with the modified Lindemann−Hinshelwood expression, and the resulting temperature dependences of F_{cent} (general center broadening factor[30]) can be represented with the following expressions:

$$F_{cent}(He) = 0.33 \exp(-T/1836\ K) + 0.67 \exp(-T/98\ K) + \exp(-3650\ K/T) \quad \text{(V)}$$

$$F_{cent}(N_2) = 0.35 \exp(-T/1864\ K) + 0.65 \exp(-T/103\ K) + \exp(-3614\ K/T) \quad \text{(VI)}$$

The average deviation of fit is 5.6%, and the maximum deviation is 21% (observed at the lowest pressure−highest temperature combination). The upper temperature limit of the rate constant parametrization is determined by the significance of non-steady-state effects[24,31−35] above 1400 K where the notion of a time-independent rate constant is inapplicable and the formalism of *virtual components*[35] must be used if an accurate description of unimolecular kinetics as a part of complex combustion kinetics is desired. Already at 1400 K, non-steady-state effects can be observed: in the case of an initial Boltzmann distribution of C_2Cl_3, the first 20% of molecules decompose with an effective rate constant that is more than twice as large as the steady-state rate constant.

IV. Discussion

The current study provides the first experimental determination of the rate constants of reaction 1. The values of k_1 were obtained as a function of temperature and bath gas density in two bath gases, helium and nitrogen. No previous experimental or computational studies of this reaction exist in the literature. Such lack of experimental and computational information is rather typical for many of the reactions involving chlorinated hydrocarbon radicals. This absence of experimental data increases the relevance of computational methods that can be used for assessing kinetic parameters. In this respect, it is interesting to compare the results of the PES study performed in the current work with the properties of the PES derived from the experiment.

The minimum energy path of reaction 1 proceeds from the nonsymmetric equilibrium structure of C_2Cl_3 through a saddle point to the shallow symmetric minimum, with subsequent departure of Cl via a symmetric pathway (Cl equidistant from both C atoms), as described in section III. This reaction mechanism is qualitatively similar to that observed for the decomposition of the CH_2CH_2Cl radical,[36,37] where the minimum energy path also passes through a symmetric bridged structure with a shallow PES well. The C_2Cl_3 PES differs from that of CH_2CH_2Cl decomposition by the existence of a saddle

point between the symmetric and the nonsymmetric configurations. It is worth noting that, although results of all calculations included in Table 2 indicate that the energy of the saddle point is higher than that of the symmetric minimum, the energy difference between these two PES critical points obtained with the highest level of calculations used, QCISD(T)/6-311+G(3df)//QCISD/6-31G(d), is only 1.4 kJ mol^{-1}. This value results, mostly, from the differences in the ZPE: the electronic energy difference is only 0.1 kJ mol^{-1}. Use of the IRCmax method[38,39] with a step size of 0.1 amu$^{1/2}$ bohr yields little change: the difference increases to 0.2 kJ mol^{-1}. These results somewhat undermine the firmness of the conclusion of the presence of the PES saddle point. Nevertheless, even if there is no maximum on the minimum energy path from the nonsymmetric to the symmetric C_2Cl_3 structure, the dynamic bottleneck of reaction 1 is likely to be located near the structure currently described as the saddle point because of the relatively large vibrational frequencies and thus low densities of states.

The values of the energy barrier (energy of the PES saddle point relative to that of the equilibrium C_2Cl_3 configuration) obtained in quantum chemical calculations are compared in Table 2 with the value derived from modeling of the experimental data. The calculated barrier values are lower than that derived from the experiment. For the higher level calculations (QCISD(T)/6-311+G(3df) single-point energy with the MP2/6-311G(2d) and the QCISD/6-31G(d) geometry optimization methods) the differences are 10.2−11.5 kJ mol^{-1}, which is outside the estimated uncertainty range of the experimental value.

Section III provides parametrization of the $k_1(T,[M])$ dependence over wide ranges of temperatures and pressures performed using the model of reaction 1 created in the current work. This parametrization is most reliable under the conditions of the experiments on the results of which the reaction model was based, that is, $T = 569-683$ K and low pressures. One should bear in mind that the model includes simplifications and that the available experimental data are not sufficient to specify all the parameters of the model. In particular, different temperature dependences of $\langle\Delta E\rangle_{down}$, average energy transferred per deactivating collision with the bath gas, will result in different values of rate constants. Also, the vibrational frequencies of the transition state were obtained in quantum chemical calculations; it was not possible to validate them against experimental information. The effect of this source of uncertainty is somewhat reduced by the fact that reaction 1 is relatively close to the low-pressure limit under most of the high-temperature conditions relevant to combustion (at atmospheric pressure and $T \geq 900$ K, $k_1°[M]/k_1^{\infty} \leq 0.14$) and thus its rate constants are less affected by the properties of the transition state than the high-pressure-limit rate constant values.

In principle, information on the reverse reaction, that of Cl addition to C_2Cl_2, can be derived from the model of reaction 1 created in the current study. Such derivation, however, requires knowledge of the enthalpy of reaction 1, information that is currently not available with the desired degree of accuracy. Therefore, we do not attempt to predict the rate constants of the Cl + C_2Cl_2 reaction in the current work.

Acknowledgment. This research was supported by the National Science Foundation, Combustion and Thermal Plasmas Program, under Grant No. CTS-0105239.

Supporting Information Available: Detailed results of the quantum chemical and rate constant calculations. This material is available free of charge via the Internet at http://pubs.acs.org.

References and Notes

(1) Tsang, W. *Combust. Sci. Technol.* **1990**, *74*, 99.
(2) Chang, W. D.; Senkan, S. M. *Environ. Sci. Technol.* **1989**, *23*, 442.
(3) Taylor, P. H.; Tirey, D. A.; Dellinger, B. *Combust. Flame* **1996**, *104*, 260.
(4) Taylor, P. H.; Tirey, D. A.; Rubey, W. A.; Dellinger, B. *Combust. Sci. Technol.* **1994**, *101*, 75.
(5) Russell, J. J.; Seetula, J. A.; Gutman, D.; Senkan, S. M. *J. Phys. Chem.* **1989**, *93*, 1934.
(6) Kostina, S. A.; Bryukov, M. G.; Shestov, A. A.; Knyazev, V. D. *J. Phys. Chem. A* **2003**, *107*, 1776.
(7) Slagle, I. R.; Gutman, D. *J. Am. Chem. Soc.* **1985**, *107*, 5342.
(8) Timonen, R. S.; Ratajczak, E.; Gutman, D.; Wagner, A. F. *J. Phys. Chem.* **1987**, *91*, 5325.
(9) Krasnoperov, L. N.; Niiranen, J. T.; Gutman, D.; Melius, C. F.; Allendorf, M. D. *J. Phys. Chem.* **1995**, *99*, 14347.
(10) Moore, S. B.; Carr, R. W., Jr. *Int. J. Mass Spectrom. Ion Phys.* **1977**, *24*, 161.
(11) Pople, J. A.; Head-Gordon, M.; Raghavachari, K. *J. Chem. Phys.* **1987**, *87*, 5968.
(12) Foresman, J. B.; Frisch, A. E. *Exploring Chemistry With Electronic Structure Methods*, 2nd ed.; Gaussian, Inc.: Pittsburgh, PA, 1996.
(13) Becke, A. D. *J. Chem. Phys.* **1993**, *98*, 1372.
(14) Lee, C. T.; Yang, W. T.; Parr, R. G. *Phys. Rev. B* **1988**, *37*, 785.
(15) Frisch, M. J.; Trucks, G. W.; Schlegel, H. B.; Scuseria, G. E.; Robb, M. A.; Cheeseman, J. R.; Zakrzewski, V. G.; Montgomery, J. A., Jr.; Stratmann, R. E.; Burant, J. C.; Dapprich, S.; Millam, J. M.; Daniels, A. D.; Kudin, K. N.; Strain, M. C.; Farkas, O.; Tomasi, J.; Barone, V.; Cossi, M.; Cammi, R.; Mennucci, B.; Pomelli, C.; Adamo, C.; Clifford, S.; Ochterski, J.; Petersson, G. A.; Ayala, P. Y.; Cui, Q.; Morokuma, K.; Malick, D. K.; Rabuck, A. D.; Raghavachari, K.; Foresman, J. B.; Cioslowski, J.; Ortiz, J. V.; Baboul, A. G.; Stefanov, B. B.; Liu, G.; Liashenko, A.; Piskorz, P.; Komaromi, I.; Gomperts, R.; Martin, R. L.; Fox, D. J.; Keith, T.; Al-Laham, M. A.; Peng, C. Y.; Nanayakkara, A.; Challacombe, M.; Gill, P. M. W.; Johnson, B.; Chen, W.; Wong, M. W.; Andres, J. L.; Gonzalez, C.; Head-Gordon, M.; Replogle, E. S.; Pople, J. A. *Gaussian 98*, revision A.9; Gaussian, Inc.: Pittsburgh, PA, 1998.
(16) Benson, S. W. *Thermochemical Kinetics*, 2nd ed.; John Wiley and Sons: New York, 1976.
(17) Robinson, P. J.; Holbrook, K. A. *Unimolecular Reactions*; Wiley-Interscience: New York, 1972.
(18) Forst, W. *Theory of Unimolecular Reactions*; Academic Press: New York, 1973.
(19) Gilbert, R. G.; Smith, S. C. *Theory of Unimolecular and Recombination Reactions*; Blackwell: Oxford, 1990.
(20) Holbrook, K. A.; Pilling, M. J.; Robertson, S. H. *Unimolecular Reactions*, 2nd ed.; Wiley: New York, 1996.
(21) Astholz, D. C.; Troe, J.; Wieters, W. *J. Chem. Phys.* **1979**, *70*, 5107.
(22) Gaynor, B. J.; Gilbert, R. G.; King, K. D. *Chem. Phys. Lett.* **1978**, *55*, 40.
(23) Bedanov, V. M.; Tsang, W.; Zachariah, M. R. *J. Phys. Chem.* **1995**, *99*, 11452.
(24) Tsang, W.; Bedanov, V.; Zachariah, M. R. *J. Phys. Chem.* **1996**, *100*, 4011.
(25) Mokrushin, V.; Bedanov, V.; Tsang, W.; Zachariah, M. R.; Knyazev, V. D. *ChemRate*, Version 1.19; National Institute of Standards and Technology: Gaithersburg, MD, 2001.
(26) Rabinovitch, B. S.; Tardy, D. C. *J. Chem. Phys.* **1966**, *45*, 3720.
(27) Knyazev, V. D.; Tsang, W. *J. Phys. Chem. A* **2000**, *104*, 10747.
(28) Feng, Y.; Niiranen, J. T.; Bencsura, A.; Knyazev, V. D.; Gutman, D.; Tsang, W. *J. Phys. Chem.* **1993**, *97*, 871.
(29) Knyazev, V. D. *J. Phys. Chem.* **1995**, *99*, 14738.
(30) Gilbert, R. G.; Luther, K.; Troe, J. *Ber. Bunsen-Ges. Phys. Chem.* **1983**, *87*, 169.
(31) Schranz, H. W.; Nordholm, S. *Chem. Phys.* **1984**, *87*, 163.
(32) Bernshtein, V.; Oref, I. *J. Phys. Chem.* **1993**, *97*, 6830.
(33) Kiefer, J. H. *Symp. (Int.) Combust., [Proc.]* **1998**, *27*, 113.
(34) Barker, J. R.; King, K. D. *J. Chem. Phys.* **1995**, *103*, 4953.
(35) Knyazev, V. D.; Tsang, W. *J. Phys. Chem. A* **1999**, *103*, 3944.
(36) Engels, B.; Peyerimhoff, S. D.; Skell, P. S. *J. Phys. Chem.* **1990**, *94*, 1267.
(37) Knyazev, V. D.; Kalinovski, I. J.; Slagle, I. R. *J. Phys. Chem. A* **1999**, *103*, 3216.
(38) Malick, D. K.; Petersson, G. A.; Montgomery, J. A. J. *J. Chem. Phys.* **1998**, *108*, 5704.
(39) Petersson, G. A. In *Computational Thermochemistry: Prediction and Estimation of Molecular Thermodynamics*; Irikura, K. K., Frurip, D. J. E., Eds.; ACS Symposium Series; American Chemical Society: Washington, DC, 1998.